

# COLOR CONSTANCY FOR LANDMARK DETECTION IN OUTDOOR ENVIRONMENTS

Eduardo Todt

Carme Torras

Institut de Robòtica i Informàtica Industrial, CSIC-UPC, Barcelona, Spain.  
todt@ieee.org, torras@iri.upc.es

## Abstract

*This work presents an evaluation of three color constancy techniques applied to a landmark detection system designed for a walking robot, which has to operate in unknown and unstructured outdoor environments. The first technique is the well-known image conversion to a chromaticity space, and the second technique is based on successive lighting intensity and illuminant color normalizations. Based on a differential model of color constancy, we propose the third technique, based on color ratios, which unifies the processes of color constancy and landmark detection. The approach used to detect potential landmarks, which is common to all evaluated systems, is based on visual saliency concepts using multiscale color opponent features to identify salient regions in the images. These regions are selected as landmark candidates, and they are further characterized by their features for identification and recognition.*

## 1 Introduction

In recent years the idea of using legged robots in environments where wheeled robots are not suitable is assuming increasing importance due to their superiority in climbing obstacles and keeping stability in irregular terrains, despite their greater complexity. Motivated by these characteristics, which are appropriate to our applications in outdoor unstructured environments, we are currently developing a prototype of a legged mobile robot [15]. A fundamental issue in this enterprise is the position estimation problem. Since, with the use of internal measures, the estimation of position accumulates errors as the robot moves, especially for walking machines in uneven terrains, it is necessary to develop location techniques based on some sort of external sensory feedback, independent of the traveled

distance [2]. Similarly as in human and animal navigation, we record visual references and use local and temporal relationships between these references in order to identify places in the world, and to plan and execute paths between locations [8]. These references are called *landmarks*, which are distinctive entities that the robot can recognize whenever they are in its detection range.

In general the characterization of landmarks in unstructured outdoor environments through some set of geometric features is not appropriate, in opposition to the case of indoor environments, since frequently the elements that could be taken as landmarks do not have well-defined shape and contours. With this assumption, landmark characterizations based on color and texture features are more reliable, because they are independent from shape.

One of the key factors that makes the detection and recognition of visual landmarks in outdoor environments a challenging task is that acquired visual information is strongly dependent on lighting geometry (direction and intensity of light source) and illuminant color (spectral power distribution), which change with sun position and atmospheric conditions. In order to overcome these adversities, the original Red, Green, and Blue (RGB) color components of acquired images are often transformed to other color spaces, in an attempt to reduce the dependence on lighting geometry and illuminant color [4][14]. This desired invariance of color representation to general changes in illumination is called color constancy.

In a previous paper [13] we presented a system for natural landmark detection in unstructured outdoor environments based on the model of human visual saliency proposed by Itti, Koch and Niebur [7]. This system had already incorporated a simple color

constancy mechanism, converting the input RGB images to chromaticity images. Although this mechanism provided some invariance to the detection of landmarks under light intensity changes, our experimental results indicated that it was necessary to search for a color constancy method more stable to the broad illumination changes observed in outdoor environments. Taking into account that mobile robot navigation and location tasks require real-time execution, the search for other color constancy methods to improve the landmark detection was done considering low computational cost as an important requirement. It is also worthwhile to remark that here the goal is to achieve a stable landmark detection system, and not to recognize colors with high accuracy.

A recent method for color constancy, which takes into account both lighting intensity and illuminant color was proposed by Finlayson, Schiele and Crowley [4]. By combining this color constancy method with color histogram comparisons, they achieved good effectiveness in object recognition tasks. Because of its independence of illuminant models, color patterns, and similarity with the chromaticity space from the first approach, their method was selected for our system. Thus, we fitted it to our landmark detection system as an image preprocessor and executed a new sequence of experiments. These experiments indicated improvements in the stability of landmark detection, but at the expense of significant additional computational cost, due to the iterative nature of the involved computation. Also this method presented the drawback of sensitivity to changes in viewpoint and to the inclusion of new objects in the scenes, because of its dependence on the global color composition of the images.

With the objective of reducing these dependencies and keeping computational cost low relative to the saliency detection task, we designed a novel algorithm for visual saliency combined with color constancy. The proposed algorithm is inspired by the color constancy model proposed by Gevers and Smeulders [5], based on the color gradients between neighboring pixels. Our approach presents the advantage that the color constancy is embedded in the visual saliency detector, instead of acting as an image preprocessor.

This paper presents an evaluation of these three different approaches to color constancy applied to our landmark detection system. First of all, the landmark detection system is described. Then, each color constancy method is explained, together with its connection to the landmark detection system, and the respective results are presented. Finally, all methods are discussed and compared between themselves.

Considering that the goal of this work is to compare different color constancy approaches applied to

landmark detection, visual saliency is computed here only based on the color information available, disregarding other relevant visual cues, like intensities and orientations, which play an important role in the complete visual saliency system [13].

## 2 Landmark detection based on visual saliency

When there is no exact knowledge of what things in the environment can be used as landmarks for the location of the mobile robot, some criterion is needed to decide which regions in the images will be considered as potentially good landmarks. Current theories of human vision indicate that potential landmark locations could be detected by using a visual saliency mechanism [3]. It has also been observed that when human perceivers are trying to build or recover the description of a scene, their attention is focused on specific relevant regions in the scene [6], which reinforces the idea of combining visual saliency techniques with landmark based location tasks for mobile robots.

In the late 19<sup>th</sup> century, the German physiologist Ewald Hering laid the foundations of the *color opponency theory*, which sustains the existence of three opponent color processes in the visual human system, constituted of red-green, yellow-blue and intensity (white-black) channels [14]. The visual saliencies in an image are proportional to the center-surround differences of the channels' responses, computed by comparing visual field regions with their respective neighborhoods. For example, red stimuli surrounded by green stimuli are considered salient, and vice versa. The same concept is also valid for blue-yellow and intensity channels. The greater the contrast between the center and surround regions, the greater the corresponding saliency. We adopt the Enroth-Cugell and Robson's model [3] of center-surround opponencies, which considers the effect of the light weighted according to the distance to the center of the receptive field by a difference of Gaussian functions.

To compute the desired color opponencies, the trichromatic input color space is transformed to an opponent color space, where it is possible to easily determine the red-green and blue-yellow opponencies. After this transformation the image is composed of four channels, each one corresponding to an opponent color. The image is then represented at eight spatial resolutions, through the use of four multiscale Gaussian pyramids, one for each channel. In these pyramids, each level is obtained by a low-pass filtering operation on the preceding level, followed by a sub sampling of factor two in each dimension. With this structure, the center-surround differences are computed by single differences between corresponding pixels at fine and coarse scales within the pyramids [7]. A center region corresponds to

a pixel at a fine scale, whereas its surround corresponds to the respective pixel at a coarser scale.

An important property of the pyramid implementation is that it facilitates opponent computations at different resolutions. By comparing centers and surrounds at high-resolution levels, e.g., between levels 2 and 5, visual saliencies of relative small targets are found, while at lower resolution levels, e.g., levels 4 and 7, relatively large salient regions are found. With this technique, it is possible to detect visual salient objects within a wide size range, for example, from small stones to big trees.

The visual saliency system builds a saliency map, which represents the distinctness of each point in an image. In this map, those points corresponding to salient areas have large values, whereas non-salient areas are indicated by small values.

The computation of center-surround differences at different scale combinations (pyramid levels 2-5, 3-6, and 4-7) results in partial visual saliency maps. The resultant partial maps are combined into a global visual saliency map, which has the cues to identify potential landmarks. This saliency map is represented at the resolution of level 1 of the pyramids, to reduce computational cost, since this level has a quarter of the number of pixels of level 0, which corresponds to the original image size. The image regions corresponding to the potential landmarks are subsequently analyzed to obtain visual signatures, capable of identifying them as an existing or a new landmark, but this is beyond the scope of this work.

### 3 Visual saliency with lighting intensity normalization

The first color constancy method we consider in this evaluation is the transformation of the *RGB* space to chromaticity coordinates (*rgb*) [14]:

$$r = \frac{R}{R+G+B} \quad (1)$$

$$g = \frac{G}{R+G+B} \quad (2)$$

$$b = \frac{B}{R+G+B} \quad (3)$$

The colors represented in *rgb* coordinates are much more stable to lighting changes than those in the *RGB* space, because the light intensity component is removed from each pixel. However, they fail to be invariant under spectral power distribution changes of the light source, because this type of perturbation affects the response of the RGB sensors in different proportions.

Following Itti, Koch, and Niebur [7] we use the opponent color space with four color components, red,

green, blue and yellow ( $R'$ ,  $G'$ ,  $B'$ ,  $Y'$ ), calculated from the *rgb* chromaticity space as follows, taking only positive values:

$$R' = r - (g + b) / 2 \quad (4)$$

$$G' = g - (r + b) / 2 \quad (5)$$

$$B' = b - (r + g) / 2 \quad (6)$$

$$Y' = (r + g) / 2 - |r - g| - b \quad (7)$$

The resulting opponent color image represented in  $R'$ ,  $G'$ ,  $B'$ , and  $Y'$  coordinates is then processed with the visual saliency system described in the preceding section. The partial saliency maps obtained from each center-surround scale (2-5, 3-6, and 4-7) and opponent color combination ( $R'-G'$ ,  $G'-R'$ ,  $Y'-B'$ , and  $B'-Y'$ ) are normalized according to their maxima and then added to form the saliency map.

There are several other definitions for opponent color spaces that could be used instead of the formulation of Itti, Koch, and Niebur [7]. For example, Swain and Ballard [11] propose similar definitions, although without a term considering the absolute difference between the  $R$  and  $G$  components to compute the yellow, while others are based on logarithmic differences, like that in Finlayson and Barends [1]. Finally, some definitions aim to obtain better decorrelation between the color components, such as those in Otha, Kanade and Sakai [10], Murrieta-Cid, Briot and Vandapel [9], and Tan and Kittler [12]. We tested all these definitions, and found the adopted formulation better than the others for our system. It is worthwhile to observe that opponent color spaces tend to decorrelate the *RGB* components, which is a desirable characteristic for pattern recognition.

We have compiled the experimental results for three scenarios subject to different real illumination conditions in Figures 1-3. The results corresponding to the lighting intensity normalization just explained are shown in the second columns of such figures. In Figure 1, it can be observed that the red roof (center left in the image), the orange flowers (center right), the brown bush (bottom left), and the yellow house (center) are indicated as salient, but the dominant green areas appear also as salient, which is not desired. Also the gravel path is salient, especially in the first image. The stability of the results to illumination changes in these images is poor.

In Figure 2, the red house (center), the yellowish bushes (bottom left and right), and the trees at the horizon line are indicated as salient. These bushes and trees are very salient and tend to reduce the relative saliency of the red house. Near the center of the second image it can be observed a spot of saliency corresponding to a red sign. The green areas in these images produce a salient background, like in Figure 1, because at a large scale (pyramid levels 3-7) they are salient relative to the sky

and near ground. In these images the stability in saliency is also poor, partly because of the inclusion of new elements in the observed scenes due to the changes in point of view, which affect the relative saliency between all the elements in each image. This effect is most noticeable in the third image, where the yellow bush is the most salient element in the scene.

In Figure 3, the green areas are dominant in the scene but they don't have opponency to other regions of similar size, like in previous figures, favorably resulting in lower background saliency. The yellow flowers (bottom right) are detected as salient, and the reddish tree is indicated as salient only in the first and third images. In the second image the RGB values of the reddish tree are too low to produce reliable chromaticity information, and thus the corresponding region is dismissed. In these images the stability of saliency is good, mainly due to a uniform background.

These results corroborate the need of looking for a color constancy method that, when incorporated in our saliency detection system, produces saliency maps more stable to illumination changes. The problem of including new salient objects, for example due to point of view changes, like in Figure 2, could be partially avoided considering separately the saliency maps for the R-G and Y-B color pairs.

#### 4 Visual saliency with lighting intensity and illuminant color normalization

In order to overcome the unfavorable sensitivity to illumination changes shown by the previous normalization, Finlayson, Schiele, and Crowley [4] proposed an algorithm for color constancy called *comprehensive color normalization*, based on iterating two types of successive color normalizations. These normalizations are aimed at removing dependence on both lighting intensity and illuminant color, in an alternate manner.

The first normalization type is the same as that defined by equations (1) through (3), transforming the image to chromaticity coordinates. The second normalization type transforms each pixel according to the global mean value of the color bands:

$$r' = \frac{1}{3} * \frac{r}{\bar{r}} \quad (8)$$

$$g' = \frac{1}{3} * \frac{g}{\bar{g}} \quad (9)$$

$$b' = \frac{1}{3} * \frac{b}{\bar{b}} \quad (10)$$

where  $\bar{r}$ ,  $\bar{g}$  and  $\bar{b}$  are the mean value of the red, green and blue bands in the whole image.

The color constancy procedure iteratively performs these two types of normalization until the dissimilarity between two successive resultant images is below an acceptance level. It is possible to demonstrate that the method converges and provides unique results, assuming that the camera sensors have a very narrow bandwidth [4]. The resulting normalized image is then converted to opponent color space, according to equations (4) through (6), and, finally, it is applied as input to the same visual saliency system described before.

Experimental results with the visual saliency detection system using comprehensive color normalization are shown in the third columns of Figures 1, 2, and 3. In Figure 1, it can be observed that the red roof (center left in the image), the orange flowers (center right), the brown bush (bottom left), and the yellow house (center) are still indicated as salient, but the dominant green areas appear also as salient, which is not desired. The gravel path presents more stability and lower saliency than in the former experiments with intensity normalization. The saliency obtained with comprehensive color normalization is outstandingly more stable to the considered illumination changes than with intensity normalization (second column), although there is an excessive saliency of green regions near the horizon.

In Figure 2, the red house (center), the yellowish bushes (bottom left and right), and the trees at the horizon line are indicated as salient. Here also the bushes and trees have high saliency, reducing the relative saliency of the red house, particularly in the third image. The spot of saliency corresponding to a red sign is also present near the center of the second image. In these images the saliency stability is enhanced compared to the intensity normalization (second column), although the same effect as before of masking salient regions due to inclusion in the image of more salient elements is noticed. Since the comprehensive color normalization uses averages of color components over the entire image, the inclusion of new salient regions affects the stability of saliency even worse than in the case of intensity normalization. This effect can be observed in the third image where the red house is no longer significantly salient.

In Figure 3 the saliency obtained through comprehensive color normalization is stable, but without significant improvement over the lighting intensity normalization.

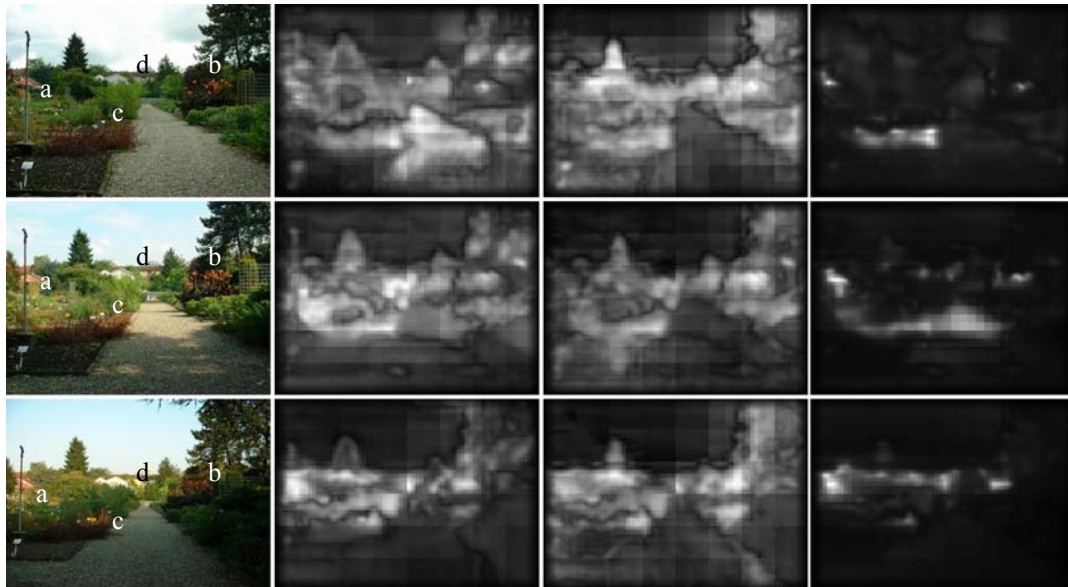


**Figure 1:** Visual saliency computed for scene “A” for three different illumination conditions (different days and times within the day). Each source image (left column) was processed with lighting intensity normalization (second column), lighting intensity and illuminant color normalization (third column), and color ratios (fourth column). The whiter regions indicate the more salient parts detected. In the source images the following things are indicated: (a) red roof, (b) orange flowers, (c) brown bush, and (d) yellow house.



**Figure 2:** Visual saliency computed for scene “B” for four different illumination conditions. Note that there are slight changes in perspective between the images. Each source image (left column) was processed with lighting intensity normalization (second column), lighting intensity and illuminant color normalization (third column), and color ratios (fourth column). The whiter regions indicate the more salient parts detected. In the source images the following things are indicated: (e) red house, (f) yellowish bushes, (g) trees, and (h) red sign. The other signs, similar in shape as the red one, are white.

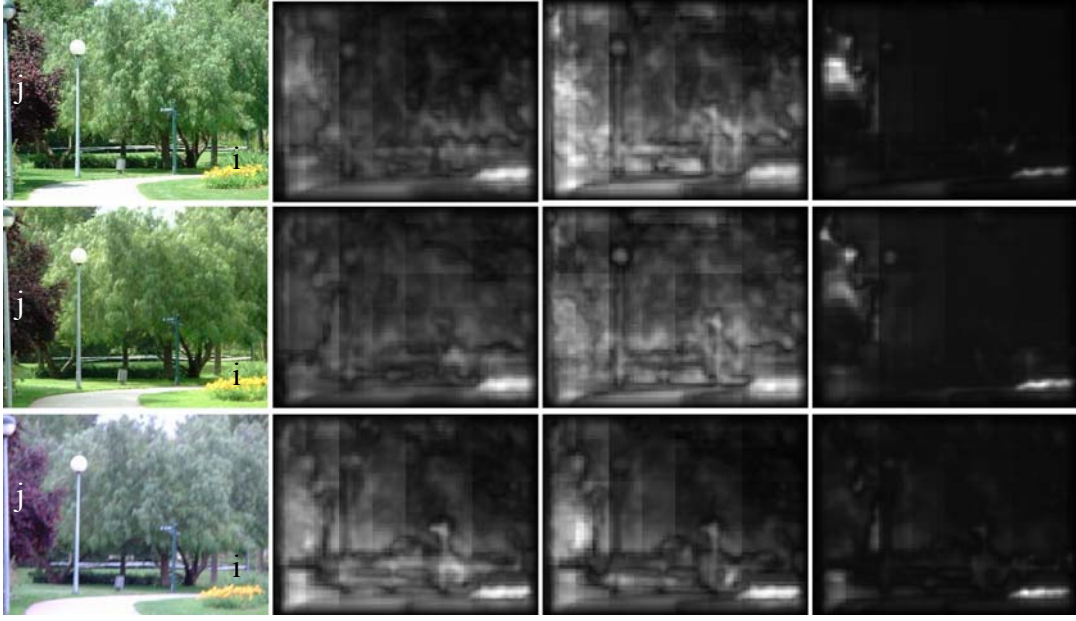


**Figure 3:** Visual saliency computed for scene “C” for three different illumination conditions. Each source image (left column) was processed with lighting intensity normalization (second column), lighting intensity and illuminant color normalization (third column), and color ratios (fourth column). The whiter regions indicate the more salient parts detected. In the source images the following things are indicated: (i) yellow flowers, and (j) reddish tree.

## 5 A new approach: visual saliency using color ratios

Gevers and Smeulders [5] show that several color representation spaces, like chromaticity  $rgb$ , saturation  $S$  and hue  $H$ , the CIE standard set of primary colors  $XYZ$ , and perceptual uniform spaces  $U^*V^*W^*$  and  $L^*a^*b^*$ , can be invariant to changes in illumination intensity, but not to changes in illuminant color. These authors propose a new color model,  $m_1m_2m_3$ , independent of the illuminant color and based on the color ratio between neighboring image locations. Assuming that the source  $RGB$  comes from narrow band sensors and that the color of illumination is locally constant, they demonstrate that their model is invariant to changes in illumination intensity and color, and also to changes of viewpoint, object geometry and illumination direction. They define the values of  $m_1m_2m_3$  for each pixel location as:

$$m_1 = \frac{R^{x_1} G^{x_2}}{G^{x_1} R^{x_2}} \quad (11)$$

$$m_2 = \frac{R^{x_1} B^{x_2}}{B^{x_1} R^{x_2}} \quad (12)$$

$$m_3 = \frac{G^{x_1} B^{x_2}}{B^{x_1} G^{x_2}} \quad (13)$$

where  $x_1$  and  $x_2$  are neighboring pixels. The authors implement the computation of neighboring pixels ratios through the determination of gradients in the logarithmic space  $\ln(R/G)$ ,  $\ln(R/B)$  and  $\ln(G/B)$ . The

maxima of the gradients are detected using a Canny edge detector, resulting in a contour image, that presents good color constancy properties.

From the definition of  $m_1$ ,  $m_2$  and  $m_3$ , we derived the idea of generalizing the concept of gradient between neighboring pixels to that of center-surround opposition. Under this approach, the  $x_1$  pixels are taken to mean center regions and the  $x_2$  pixels correspond to surround regions. Then, we define the center-surround color opponencies based on color ratios:

$$RG = \frac{R_c G_s}{R_s G_c} \quad (14)$$

$$GR = \frac{R_s G_c}{R_c G_s} = \frac{1}{RG} \quad (15)$$

$$BY = \frac{B_c Y_s}{B_s Y_c} \quad (16)$$

$$YB = \frac{B_s Y_c}{B_c Y_s} = \frac{1}{BY} \quad (17)$$

where  $R$ ,  $G$ ,  $B$ , and  $Y$  are red, green, blue and yellow center or surround regions, according to the subscript. The  $RG$  opponency corresponds to a visual field that is excited by red stimuli in the center and by green stimuli in the surround, and inhibited by red stimuli in the surround or green stimuli in the center. The  $GR$  corresponds to the converse. The same consideration is valid for the  $B$  and  $Y$  color pair. With the use of centers and surrounds at different scales, located at coarser or

finer levels in the Gaussian pyramids, it is possible to compute the color opponencies at multiple scales.

It is important to observe that in the previous visual saliency system the saliencies were proportional to the differences between center and surround regions, and here they are proportional to the ratios of these regions. Like Gevers and Smeulders [5] we use the logarithms of the spaces  $(R/G)$  and  $(Y/B)$ , so we can compute the opponencies by differences of logarithms across the scales, instead of divisions. Additionally, as the logarithm of the inverse of an expression is a simple inversion of sign, we have only two pyramids for color, one for  $\ln(R/G)$  and the other for  $\ln(Y/B)$ , saving the computation of  $\ln(G/R)$  and  $\ln(B/Y)$  pyramids.

The proposed color constancy/visual saliency algorithm, based on multiscale color ratio, consists of the following steps:

1. Conversion from input  $RGB$  space to opponent color space  $R'G'B'Y'$ , using equations (4) to (7).
2. Construction of the  $\ln(R'/G')$  and  $\ln(Y'/B')$  Gaussian pyramids, with 8 scale levels.
3. Computation of the multiscale color ratios with differences of logarithms at pyramid levels 2-5, 3-6, and 4-7.
4. Normalization of partial results through exponentiation (inverse of logarithm) and composition of a resultant saliency map with the sum of all partial results.

In the implementation of this algorithm the  $\ln(R'/G')$  and  $\ln(Y'/B')$  are computed as  $\ln(R') - \ln(G')$  and  $\ln(Y') - \ln(B')$ . Indeterminations are avoided by taking  $\ln(0)=0$ . The partial saliency maps obtained from each center-surround scale (2-5, 3-6, and 4-7) and opponent color combination ( $R'-G'$ ,  $G'-R'$ ,  $Y'-B'$ , and  $B'-Y'$ ) are normalized through exponentiation before combining them to form the saliency map. Since this operation is the inverse of the logarithm applied to the source signal, it restores the linear proportion between the partial maps.

Experimental results obtained with the multiscale color ratio algorithm are shown in the fourth columns of Figures 1, 2, and 3. In Figure 1, a better stability than using the former approaches is observed, although in the second and third images remains some instability from the greenish-yellowish trees and the yellowish gravel path.

In Figure 2 the results are also more stable than the intensity normalization and comprehensive color normalization ones, with the exception of the first image, where the yellowish bushes are not indicated as salient. In Figure 3 the results are also stable, although the reddish tree is not indicated as salient in the third

image. This effect is due to the fact that the saliency of the yellow flowers is approximately ten times higher than the saliency of the tree. This masking effect could be avoided by considering separately the saliency maps of  $R'-G'$  and  $Y'-B'$  opponencies.

## 6 Performance comparison

As a benchmark evaluation, we applied the three techniques to a source  $RGB$  image of 512x384 pixels, using a PC computer, with an AMD Athlon 800MHz processor, 128Mb DRAM, under Windows 98, averaging 100 successive executions of each approach. Table 1 shows the execution times obtained, where saliency detection with our multiscale color ratio method presents lower execution time than the other approaches.

Table 2 shows the distribution of computing time between the most important tasks carried out by the proposed algorithm. The computation of center-surround differences is only 8% of the total execution time, because these differences are computed at the scale of the centers, instead of at the source image scale. For example, for a 512x384-pixel image, the center-surround differences between levels 3 and 7 are computed using the dimensions of the center image at the level 3 of the pyramids, i.e., 64x48 pixels.

It can be observed that the task of initializing data structures represents a significant computational effort in the processing of visual saliencies. The better performance of the multiscale color ratio algorithm compared to the others is due to the fewer float operations necessary to compute the saliency, although the introduction of the logarithm operation is significant in the overall execution time.

**Table 1:** Execution times for computing visual saliency with the three different approaches.

Approach	Seconds
Intensity normalization	0.86
Comprehensive color normalization	1.19
Multiscale color ratio	0.77

**Table 2:** Distribution of execution time between the tasks performed within the multiscale color ratio approach.

Task	Fraction of total execution time
Conversion RGB to $R'G'B'Y'$	0.21
Logarithm of $R'G'B'Y'$	0.22
Pyramids $\ln(R'/G')$ , $\ln(Y'/B')$	0.23
Center-surround differences	0.08

## 7 Conclusions

In this paper we have compared three approaches to color constancy as applied to a landmark detection system based on opponent-color saliency.

The first approach, lighting intensity normalization through the transformation of color from *RGB* to chromaticity space, has the drawback of producing a loss of some information, since it projects colors onto a lower dimensional space. More specifically, since each of the normalized colors is linearly dependent, only two of the normalized colors (e.g., *r* and *g*) are enough to represent the *rgb* space. Although this method is simple, it has shown an undesirable sensitivity to shadows and changes in the illuminant color.

The comprehensive color normalization has proven to be more stable to illumination changes than the lighting intensity normalization, but presents higher computational cost and also produces undesired changes in the detected salient regions. The color constancy is affected by the global color measures in the image, and so the method is sensitive to the inclusion/exclusion of objects in the scenes.

We conclude that, for the target application, our method is more suitable than the other, because it presents stable results with better correspondence of saliency to the image regions that that we want to use as landmarks in outdoor environments. This characteristic is obtained with an efficient algorithm, which presents a slight improvement in performance compared to the other approaches.

## Acknowledgments

This work is partially supported by the Spanish Science and Technology Commission (CICYT), in the scope of the project "Autonomous navigation of robots guided by visual targets", grant DPI2000-1352-C02-01.

## 8 References

- [1] Berens, J. and Finlayson, G.D., "Log-opponent chromaticity coding of colour space", 15th International Conference on Pattern Recognition, Barcelona, Spain, 2000, vol. 1, pp.206-211.
- [2] Berns, K.; Kepplin, V. and Dillmann, R. "Terrain and obstacle detection for walking machines using a stereo-camera head", 24th Annual Conference of the IEEE Industrial Electronics Society, 1998, IECON '98, pp.1170-1175.
- [3] Bruce, V., Green, P.R., and Georgeson, M.A., Visual Perception, Psychology Press, United Kingdom, 1997.
- [4] Finlayson, G.D., Schiele, B., and Crowley, J.L. "Comprehensive colour image normalization", 5th European Conference on Computer Vision, 1998, pp.475-490.
- [5] Gevers, T. and Smeulders, A.W.M., "Color-based object recognition", Pattern Recognition, 32(3), 1999, pp.453-464.
- [6] Grossberg, S., Mingolla, E., Ross, W., "A neural theory on attentive visual search: interactions of boundary, surface, spatial, and object representations", Psychological Review, 101(3), 1994, pp.470-489.
- [7] Itti, L., Koch, C., and Niebur, E., "A model of saliency-based visual attention for rapid scene analysis", IEEE Transactions on Pattern Analysis and Machine Intelligence, 20(11), 1998, pp.1254-1259.
- [8] Levitt, T.S. and Lawton, D.T., "Qualitative Navigation for Mobile Robots", Artificial Intelligence 44, 1990, pp.305-360.
- [9] Murrieta-Cid, R., Briot, M., and Vandapel, N., "Landmark identification and tracking in natural environment", LAAS Report #98037, Toulouse, France, January 1998.
- [10] Otha, Y., Kanade, T., and Sakai, T., "Color information for region segmentation", Computer Graphics and Image Processing, 13, 1980, pp.222-241.
- [11] Swain, M.J. and Ballard, D.H., "Color indexing", Int. Journal of Computer Vision, 7(1), 1991, pp.11-32.
- [12] Tan, T.S.C. and Kittler, J., "Colour texture analysis using colour histogram", IEEE Proceedings of Vision Image and Signal Processing, 141(6), 1994, pp.403-412.
- [13] Todt, E. and Torras, C., "Detection of Natural Landmarks through Multiscale Opponent Features", 15th International Conference on Pattern Recognition, Barcelona, Spain, 2000, vol. 3, pp.988-991.
- [14] Wyszecki, G. and Stiles, W.S., Color Science: Concepts and Methods, Quantitative Data and Formulae, John Wiley and Sons, U.S.A., 1982.
- [15] Institut de Robòtica i Informàtica Industrial, CSIC-UPC, Barcelona, Spain, "The Argos robot", 2001, [www-iri.upc.es/people/porta/robots/argos](http://www-iri.upc.es/people/porta/robots/argos).